


Article

Investigation of Structural and Optical Characteristics of Biopolymer Composites Based on Polyvinyl Alcohol Inserted with PbS Nanoparticles

Ari H. A. Darwesh ¹, Pshko A. Mohammed ², Soran M. Mamand ¹, Sarkawt A. Hussien ¹, Shujahadeen B. Aziz ^{1,3,*} , Mohamad A. Brza ⁴, Ranjdar M. Abdullah ¹ and Wrya O. Karim ⁵

¹ Hameed Majid Advanced Polymeric Materials Research Laboratory, Physics Department, College of Science, University of Sulaimani, Qlyasan Street, Sulaimani 46001, Iraq

² Charmo Research Center, University of Charmo, Peshawa Street, Chamchamal 46023, Iraq

³ The Development Center for Research and Training (DCRT), University of Human Development, Sulaymaniyah 46001, Iraq

⁴ Department of Physics, College of Science, University of Charmo, Chamchamal 46023, Iraq

⁵ Department of Chemistry, College of Science, University of Sulaimani, Qlyasan Street, Sulaimani 46001, Iraq

* Correspondence: shujahadeenaziz@gmail.com

Abstract: The film casting method is implemented to synthesize a series of films consisting of polyvinyl alcohol (PVA) films and 4 wt%, 8 wt%, and 12 wt% lead sulfide (PbS) nanoparticles (NPs). X-ray diffraction (XRD), Fourier-transform infrared spectroscopy (FTIR), and Ultraviolet-visible (UV-vis) spectroscopy were used to ensure the impact of PbS loading on PVA properties, particularly optical ones. The FTIR results show a decrease in the intensity for all the bands and the XRD results show different features for the composites from that of the pure PVA. The optical properties, including optical transmission, surface reflection, and absorption, were investigated. Additionally, the significant optical parameters, for instance, the dielectric nature and refractive index of the films, were analyzed. The findings have shown that PbS NPs in the PVA films decrease UV and visible transmission through polymer composites and increase their ability to reflect the incident light. Tauc's equation is applied to determine the optical bandgap energy (E_g) and verify whether it is direct or indirect. Using the relation between photon energy and optical dielectric loss, the E_g was measured and the type of electron transition was measured, which eases the exponent value (γ) specification from Tauc's method. The E_g decreases from 6.3 eV to 5.25 eV when PbS NPs are added. The refractive index is improved from 1.27 to 2.16 for the polymer nanocomposite (NCPs) film with optimum PbS NPs. Then, the Wemple–DiDomenico model corresponding to a single oscillator is applied to the dispersive medium to determine the refractive index dispersion. Both the dispersive energy (E_d) and single-oscillator energy (E_o) are evaluated accurately. Moreover, the variation of both real and imaginary parts of the dielectric constant of polymer films were studied. Finally the optical parameters such as charge density, dielectric constant at high frequencies, optical mobility (μ), angular frequency (ω_p), optical resistivity (ρ), and relaxation time (τ) of electrons are shown quantitatively. The ω_p of the electron is increased from 1.06×10^{29} to 81.5×10^{29} Hz when the PbS NPs is added. The μ of the electrons is also increased from 4.85 to 6.22 $\text{cm}^2/(\text{V}\cdot\text{s})$ by adding the PbS NP.

Keywords: PVA biopolymer; nanocomposite; XRD and FTIR analyses; optical properties; energy band gap



Citation: Darwesh, A.H.A.; Mohammed, P.A.; Mamand, S.M.; Hussien, S.A.; Aziz, S.B.; Brza, M.A.; Abdullah, R.M.; Karim, W.O. Investigation of Structural and Optical Characteristics of Biopolymer Composites Based on Polyvinyl Alcohol Inserted with PbS Nanoparticles. *Coatings* **2023**, *13*, 578. <https://doi.org/10.3390/coatings13030578>

Academic Editor: Alexandre Botas

Received: 7 January 2023

Revised: 28 February 2023

Accepted: 2 March 2023

Published: 7 March 2023



Copyright: © 2023 by the authors. Licensee MDPI, Basel, Switzerland. This article is an open access article distributed under the terms and conditions of the Creative Commons Attribution (CC BY) license (<https://creativecommons.org/licenses/by/4.0/>).

1. Introduction

The synthesis of inorganic nanoparticles (NPs), as one of the hottest topics in the literature, has drawn many researchers over the last decade. This is owing to numerous unique characteristics; for example, thermal conductivity and optical and magnetic properties. In

addition, several other characteristic properties, such as high surface, quantum tunneling effect, quantum size impact, interface effects, and catalysis, are considered [1]. On the other hand, an organic material involved in the study of nanoscience occupies an indispensable position since it offers cost-effective processing and trouble-free incorporation into inorganic materials. For example, an attempt to improve the qualities of plastics is carried out by combining several influential properties such as high optical cross-sections, efficient nonlinear responses, and their broadband tunability in organics, which in turn makes the final products eligible for applications [2]. A tremendous focus has been devoted to improving the electrical and optical properties of polymers. The mechanics of charge transport in polymer materials must be thoroughly understood in order to achieve this purpose. Consequently, in order to enhance reflection, antireflection, interference, and polarization, researchers have extensively studied electrical conduction and optical characteristics [3].

To date, fast advancement in material science has been witnessed; in particular, nano-materials thin film preparation occupies the literature [4]. The PbS is often synthesized at the nanoscale and is in use as one of the materials with a narrow E_g of 0.41 eV. It is desirable as an IV-VI group of semiconductors widely used in many sectors, such as thermoelectric technologies, solar cells, infrared, and photovoltaic devices. Mamiyev and Balayeva [5] described the PbS NPs properties' technological importance as the foundation of modern semiconductor optoelectronics. The authors documented that the PbS has shown an outstanding versatility and great promise for applications in both conventional optical devices and the new generation of nano-optoelectronics and nano-electronics owing to their specific structure and size-related properties.

Melnikov et al. [6] described how one of the solutions to improve the properties of polymers is by adding NPs to fabricate polymer-based Nanocomposites (NCPs). These properties include adjustable electrical and thermal conductivity, the capability of making a developed inner surface, increased durability and mechanical strength, and many others. The authors reported that the materials formed can have several applications, for example packaging, renewable energy sources, smart materials, biomimetic materials and technologies, etc. John, B. [7] reported that polymer NCPs have a key role in modern day life and have been broadly studied for wide properties which make them appealing to various applications, for instance electrochemical sensors and biosensors.

Polymers currently offer brilliant host materials which involve inorganic particle incorporation. The most popular and usable polymer is PVA, which is the most attractive because it has hydroxyl functional groups, is cheap, and is widely available [8,9]. After selecting a proper nano-filler (NOF), controlling its concentration [10], and managing how the particles are dispersed and the manner of interacting with the polymer host, the optical properties could be improved considerably [11,12]. This is considered a dramatic modification to the pure polymer properties. All the desired properties of polymer material, such as thermal stability [13], strong charge storage, high flexibility, low electrical conductivity, and high dielectric strength, exist in PVA [14]. It is a synthetic polymer possessing the desired physical, chemical, and film-forming capabilities. Furthermore, it is benign and water-soluble. The eligibility of PVA polymers for open exploitation has captivated the attention of many researchers. PVA has a carbon chain backbone structure with hydroxyl (OH) groups attached to methane carbons [15,16]. These OH groups provide hydrogen bonding, which facilitates the development of polymer composites [1]. From a practical standpoint, nano-filled polymers as hybrid materials gather all the desired properties of the polymer and the filler to produce substrates for microwaves [17], an electrolyte for fuel cells [18], an adsorptive photocatalyst [19], a supercapacitor [20], and humidity sensors [21].

The current study examines the impact of various PbS NPs on the structural and optical characteristics of PVA films. From the UV-vis analysis, one can acquire optical energy gap diagrams and optical parameters that are relatively influenced through processing conditions.

2. Experimental Method

2.1. Sample Preparation

The PVA with MW 89,000–98,000 hydrolyzed in pure form and PbS NPs were the primary raw materials provided by Sigma-Aldrich. The solution cast method was carried out to synthesize the PVA-based polymer NCPs films. In the synthesis of NCPs, the first step started with the dissolving of 1g of PVA powder in 100 mL of distilled water and stirring with a magnetic stirrer for around 3 h at 70 °C. Afterwards, the solution was allowed to cool down for 24 h. Subsequently, different portions of PbS NPs (4, 8, and 12 wt%) were added to a series of previously prepared solutions and stirred for 15 min. Beyond 2 min, a homogenous solution was obtained with the Cole-Parmer CPX-750 ultrasonic processor. The products were converted to a state that was free from solvent by remaining gently in the containers for two weeks and casting several plastic Petri dishes at room temperature. The components in each labeled sample are presented quantitatively in Table 1.

Table 1. Chemical elements of PVA/PbS.

| PbS (g) | Films | PVA (g) | PbS wt% |
|---------|-------|---------|---------|
| 0.0000 | PC-0 | 1 | 0 |
| 0.0417 | PC-4 | 1 | 4 |
| 0.0870 | PC-8 | 1 | 8 |
| 0.1360 | PC-12 | 1 | 12 |

2.2. Physical Measurements

At room temperature, an X-ray diffractometer (model Empyrean-Panalytical) was used to measure the polymer film's X-ray diffraction (XRD). The voltage and current were set at 40 kV and 45 mA, respectively. The scanning was conducted using a monochromatic X-ray beam with 1.5406 \AA through the entire surface of the samples, while the glancing angle was adjusted accurately at $10^\circ \leq 2\theta \leq 70^\circ$. A spectrophotometer (Perkin Elmer, Melville, NY, USA) was used to acquire the FTIR spectra. Within $500\text{--}4000 \text{ cm}^{-1}$, the FTIR spectra for all films were recorded at a resolution of 2 cm^{-1} . A Jasco V-570 UV-Vis-NIR spectrophotometer (Jasco SLM-468, Tokyo, Japan) in absorbance mode was used to measure the ultraviolet-visible (UV-vis) absorption spectra of the composite films. Regarding FTIR and the UV-Vis tests for the samples, firstly the FTIR and UV-Vis spectroscopy devices without any samples were corrected for background and then the FTIR and UV-Vis spectra were measured for the samples.

3. Results and Discussion

3.1. Structural Properties of Polymer Composites

3.1.1. XRD Pattern Analysis

The structural study of the polymer treated with PbS NPs was analyzed using XRD. The PVA and the PbS-loaded PVA were studied using XRD to identify the structures' changes, as shown in Figure 1. It was noticed that the intensity of the XRD peak of PVA at $2\theta = 19.6^\circ$ decreased with increasing PbS. The XRD peaks of PbS NPs at 26.15° , 30.35° , 43.35° , and 51.1° appeared in the NCPs films [22]. The strong intramolecular hydrogen bonds and intermolecular interactions between PVA polymer chains decreased crystallinity. As seen in Figure 1, the intensity of the XRD peak for pure PVA (PC-0) at $2\theta = 19.6^\circ$ was decreased and broadened when PbS NPs was added, meaning that the crystallinity decreased in the NCPs samples. This would be due to the electronic interactions between the functional groups of PVA and PbS NPs that cause the disruption of the hydrogen bonds which bind the PVA polymer chains together [13,23,24]. The extra XRD peaks emerged in the NCPs samples due to adding the PbS NPs. The interesting thing to notice in the XRD of the NCPs samples is the appearance of an extra diffraction peak. The XRD pattern of PbS NPs is shown in refs. [24,25]. The XRD peaks at 2θ values of 26° , 30° , 43° , 51° , 53° , 63° , and 69° correspond to the (1 1 1), (2 0 0), (2 2 0), (3 1 1), (2 2 2), (4 0 0), and (3 3 1)

planes, respectively [25]. The Debye–Scherrer equation can be determined using the crystal size [26]:

$$D = \frac{K\lambda}{\beta \cos\theta} \quad (1)$$

where β is the FWHM, λ is the incident beam wavelength, K is the proportionality constant, which is 0.9 [26], and D is the particle size. Noticeably, a broad FWHM (β) and smaller crystallite sizes are recognized by the broader peaks [27]. The diffraction peak ($2\theta = 30.35^\circ$) was used to measure the crystals' average size, which is about 26.59 nm.

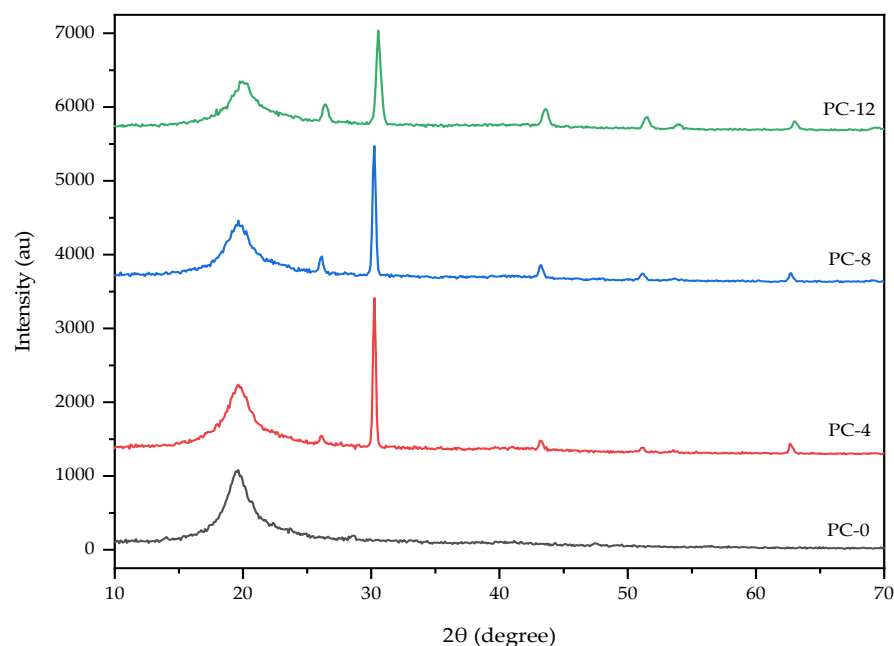


Figure 1. The pattern of XRD for pure PVA and PVA/PbSNCPs.

3.1.2. FTIR Analysis

FTIR spectroscopy can record the functional groups used as a fingerprint for recognizing the chemical structure and the extent of molecular interaction of the PbS-NPs and pure PVA. To confirm the effect of the dopant on the PVA structure, the FTIR of PVA, PbS NPs, and PVA/PbS NCPs were measured as shown in Figure 2. The stretching and bending vibrations of the C-H, C-C, C-O, and O-H bonds are the primary features of PVA. In particular, the O-H stretching vibration formed a broad and robust band centering at 3280 cm^{-1} [28,29]. The detected peak of the bond between the PVA and -OH group shifted to a lower wavenumber, indicating an electrostatic interaction between the -OH groups and PbS NPs [30–32]. The PVA/PbS NCPs of the FTIR spectra show weak bands, indicating a complexation among PbS NPs and PVA molecular chains [28].

3.2. Optical Properties

3.2.1. UV-Visible Absorption and Transmittance

Once the polymer is doped with PbS NPs, drastic modification in the optical response will occur. Accordingly, optical band gap energy (E_g) using UV-vis spectroscopy can be measured. Then, based on the molecular orbital theory, one can know how electrons in the π , n , and σ -orbitals are promoted from the lower ground level to the higher levels once they absorb the light by incident beam spectral range from ultraviolet to the visible region [33].

The optical spectra corresponding to PVA and PVA-loaded samples are shown in Figure 3. The samples have a small absorption in the spectral range from 350 to 800 nm. The only absorption peak at the short UV region is attributed to the absorption of the photon energy that is adequate to interact with atoms of the polymer material, resulting in transferring some electrons from the valence to the conduction band. The incident light

transmits completely through the pure PVA. The transmittance decreases as the additive filler amount are increased [34]. For example, the PVA containing 12 wt% of PbS NPs shows about 74% transparency. This shows that, even though a significant amount of the filler was added to the polymer, the NCPs still have good transparency in the visible region with a strong UV absorption.

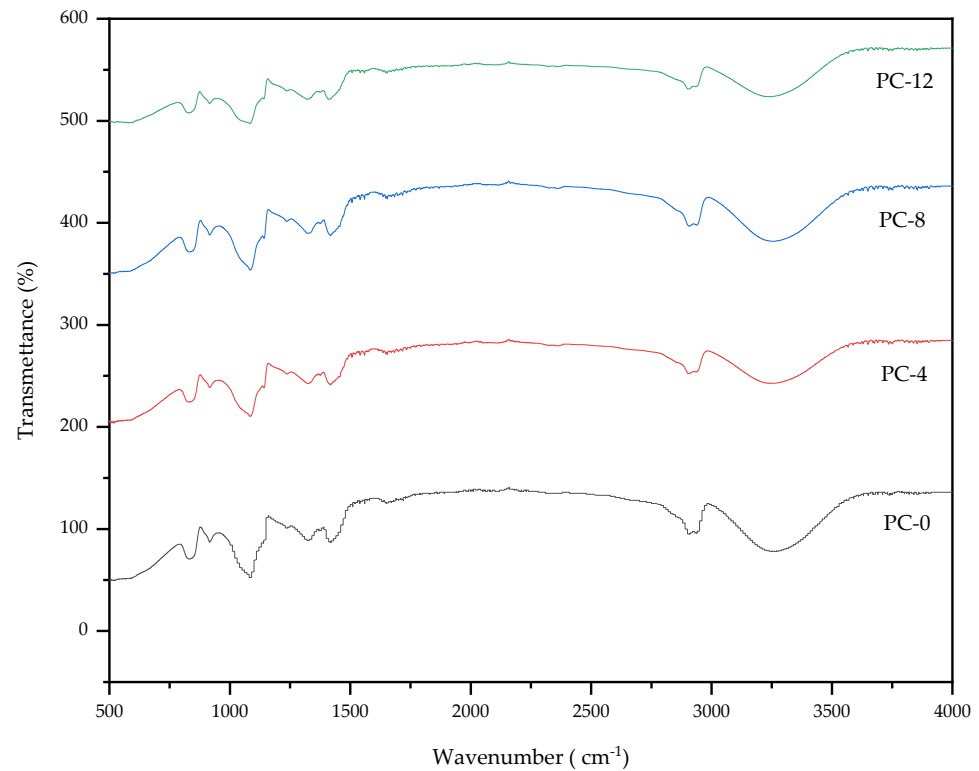


Figure 2. FTIR spectra associated with PVA/PbSNCPs and PVA.

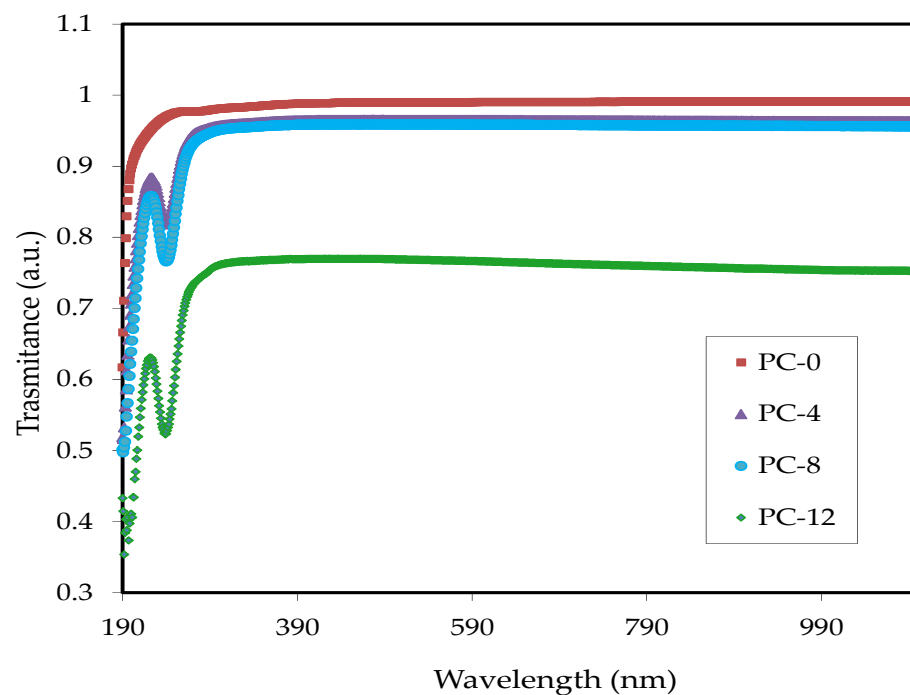


Figure 3. Transmittance spectra associated with PVA and PVA/PbS.

In the absorption process, when a sample is illuminated, the amount of light that is transmitted into the system is determined using Equation (2). The absorbance, A , or quantity of light absorbed can mathematically be shown as follows:

$$A = -\log \left[\frac{I}{I_0} \right] \quad (2)$$

where I_0 and I stand for the initial beam intensity and the intensity of light passing through the sample, respectively [35,36]. The optical absorption spectra corresponding to PVA and PVAs loaded with various PbS NPs over the broadband range from 190 to 900 nm can be manipulated, as shown in Figure 4. The absorption peaks in the spectra inversely and proportionally change with increasing wavelength and increasing PbS NPs content. The apparent peak that is characteristic appears in the UV region. Remarkably, the doped PVA possesses a tunable UV absorption region. As stated previously, according to the molecular orbital theory, when UV light is absorbed, electrons in the π , σ , and n -orbitals are strongly jumped from the lowest energy state to the higher excited states; therefore, the $\pi \rightarrow \pi^*$, $n \rightarrow \pi^*$, and $\sigma \rightarrow \sigma^*$ transitions will occur. With those transitions, most optical transitions in the visible region are produced by contaminants. Figure 4 displays the 240 nm peak caused by $n \rightarrow \pi^*$ transitions [37]. The transparency of the samples at relatively higher wavelengths is observed. The spectrum of PVA contains an absorption edge near 210 nm, and the absorption edge of the spectra of all the doped samples slightly shifts towards the longer wavelength. The $\pi \rightarrow \pi^*$ transition is an electronic transition which belongs to the conjugated (C=O) group. Moreover, it can be connected to the absorption band in all the systems in the spectral range from 200 to 300 nm. Furthermore, both the non-doped and doped samples had a small absorption band around 330 nm, which is a vibrational feature of PVA. As an interesting phenomenon, the vibronic shoulder appears as the PbS NP concentration increases. This establishes a relationship between the vibronic absorption band and the growth of the crystalline components in the systems. The similar shapes in the absorbance spectra of the PVA:PbS confirm reaching a desired homogeneity throughout the film preparations [13,38].

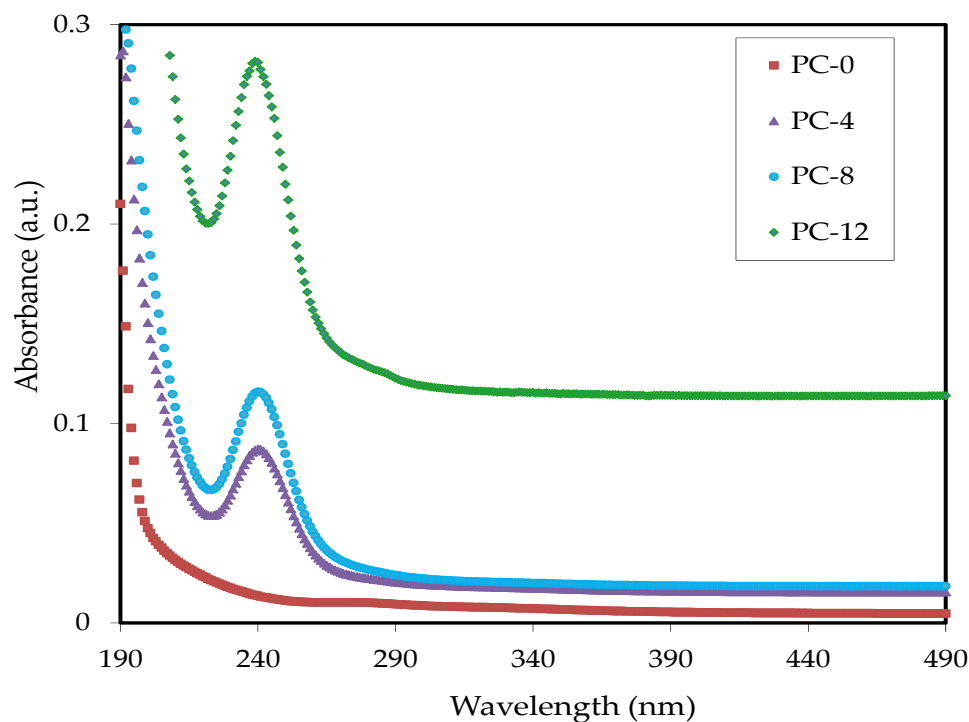


Figure 4. Absorption spectra over UV and the short visible region corresponding to PVA and PVA-loaded samples.

3.2.2. Coefficient of Absorption and Absorption Edge Study

The optical absorption coefficient can determine the material's ability to absorb light. The analysis of optical properties is a method to determine vibrational energy bands and electron transitions between different energy states [39]. Additionally, a comprehensive understanding of the absorption mechanisms can predict materials' optically induced crystallinity and non-crystallinity. The extensive examination of the optical property shows developments in the energy band structure modifications. From the analysis of optical absorption spectra taken for the systems, the energy gap (E_g) is measured. By considering the transmittance and reflectance in the calculation, the following relationship can be used to determine the absorption coefficient (α) [40]:

$$\alpha = \frac{1}{t} \ln \left[\sqrt{\frac{(1-R)^4 + 4T^2R^2 - (1-R)^2}{2TR^2}} \right] \quad (3)$$

where T , t , R , and α are the transmittance, thickness, reflectance, and absorption coefficient, respectively.

The value of T is derived from Beer's law ($T = 10^{-A}$). Two main phenomena occur through transmissions: light transmitted by the guiding medium and absorption. The response of a material to the incident light is proportional to the total absorbance of radiation intensity I_A , reflected radiation intensity I_R , and transmitted beam I_T as the radiation passes through the medium, as seen in Equation (4):

$$I_0 = I_R + I_A + I_T \quad (4)$$

The radiation intensity is measured in W m^{-2} , which describes the total energy transmission per unit of time per area. Equation (4) can also be shown as:

$$R + A + T = 1 \quad (5)$$

where R shows reflectivity (I_R/I_0), A stands for the absorptivity (I_A/I_0), and T is the transmittivity (I_T/I_0). The other symbols are T , A , and R , representing transmittance, absorbance, and reflectance, respectively. The study of optical absorption shows that the absorption edge as a key factor is used to show the electronic structure of the materials. The occurrence of the indirect and direct transitions inside the bandgap (BG) is clarified from the optical absorption spectra [40].

Figure 5 shows the optical coefficient of absorption as a function of the energy of photons of the PVA and PVA:PbS films. Upon the addition of PbS NPs, the absorption edges of PVA shift toward lower photon energy. The shifting is evidence of reducing the optical E_g due to the additive materials. Table 2 summarizes the absorption edges measured by extrapolating the linear parts of the absorption coefficient versus photon energy.

Table 2 shows that by increasing the PbS amount, the absorption edge decreased. This decrease occurs due to creating new localized states in the bandgap. In other words, the transition lies below the PVA energy gap and expands the bandgap's tail. The Urbach tail's (UT) width measures the degree of disorder in the forbidden gap and the degree of defective levels. The following equation can be used to calculate the UT width [38]:

$$\alpha = \alpha_0 \exp(h\nu/E_U) \quad (6)$$

where α_0 is a constant and E_U is the Urbach energy.

Table 2 reveals an overview of the band tail values of both PVA and PVA-loaded samples. The band tail values were determined from the inverse of the slopes associated with the lines given in Figure 6. It has been emphasized that the E_U values increase as the PbS NPs amount is increased. The consequence of increasing the values produces tail-to-tail transitions, and it is an indication of the newly constructed localized states with relatively high density [8,41].

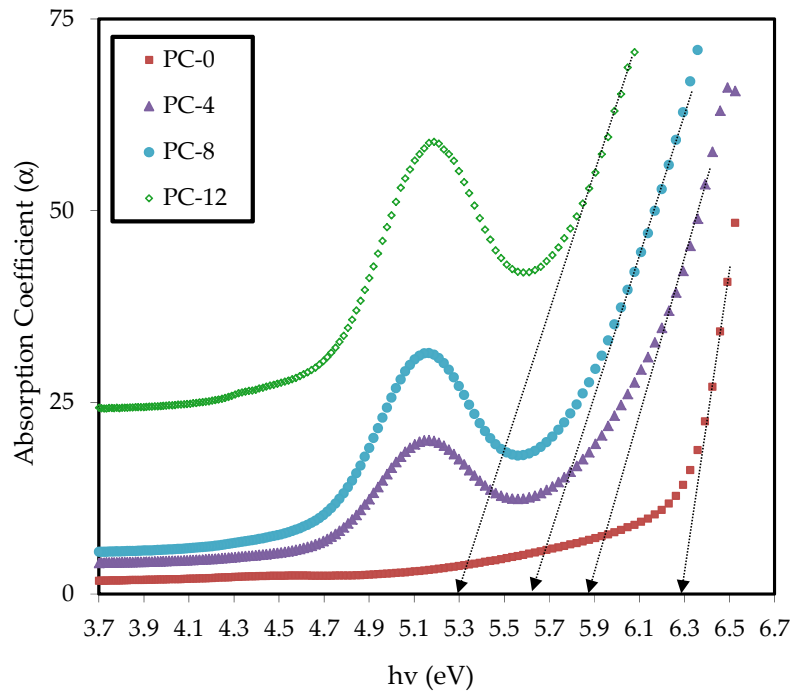


Figure 5. Absorption coefficients as a function of photon energy for all the polymer composite samples.

Table 2. Extracted Urbach tail localized state and optical absorption edge; the magnitudes have approximately been determined from Figure 5.

| Films | Absorption Edge (eV) | E_U (eV) |
|-------|----------------------|------------|
| PC-0 | 6.3 | 0.20 |
| PC-4 | 5.88 | 0.62 |
| PC-8 | 5.67 | 0.58 |
| PC-12 | 5.3 | 1.30 |

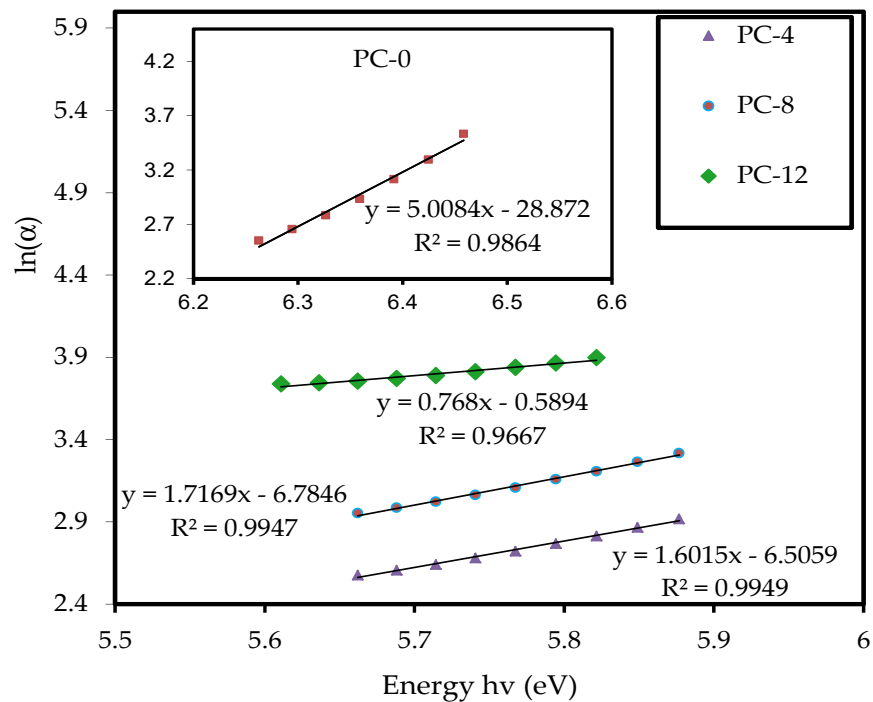


Figure 6. Urbach plot for pure PVA and PVA/PbS NCPs.

3.2.3. Study of Optical Band Gap Energy and Dielectric Loss

As a common approach, UV-vis spectroscopy is applied to measure the E_g of materials. The electrons will excite due to photon energy absorption, leading to absorption edge modification. Consequently, some deviations will occur in the BG, which facilitates the determination of optical band gap energies [39].

Figure 7a–d depict the plot of $(\alpha hv)^{\frac{1}{\gamma}}$ with photon energy (hv) and for all the systems. The values of E_g of the samples also can be determined using the ϵ_i approach. The optical E_g is obtained from the Tauc’s equation using Equation (7) [42–44].

$$\alpha hv = B(hv - E_g)^\gamma \tag{7}$$

where B is a constant parameter related to the formation of new energy bands, and E_g represents the optical E_g . The γ could take the values of 1/2 and 3/2, which indicate the electron transitions of direct allowed and forbidden, respectively. The γ can also take the values of 2 and 3, which refer to indirect allowed and forbidden transitions, respectively.

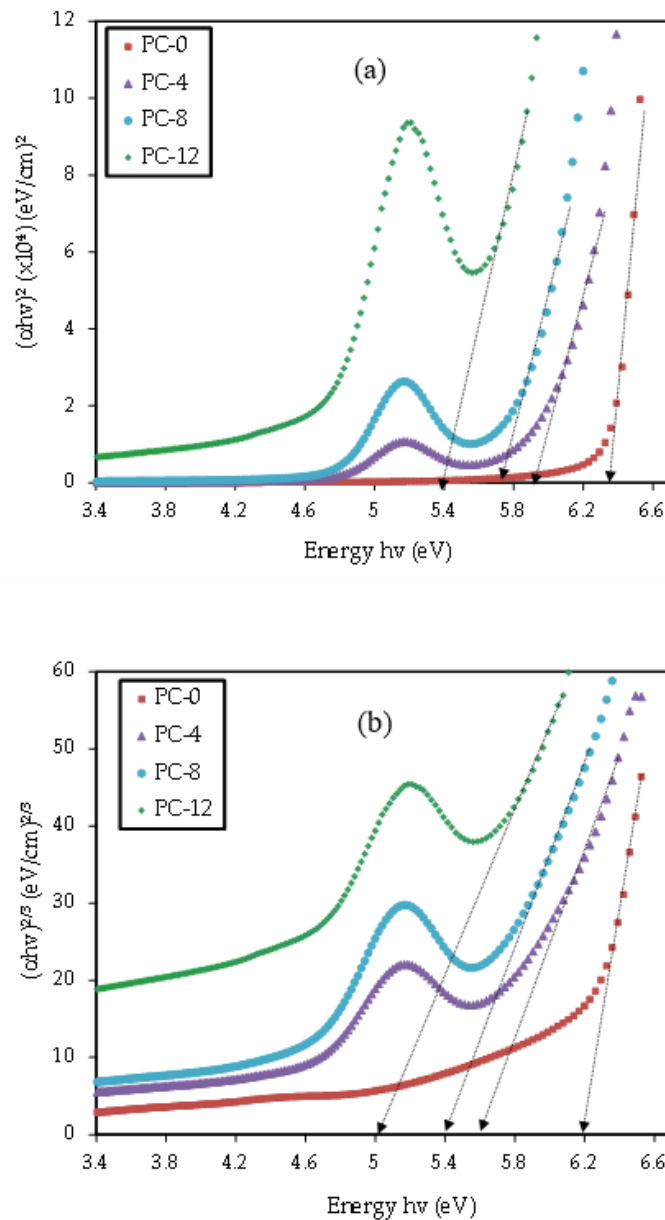


Figure 7. Cont.

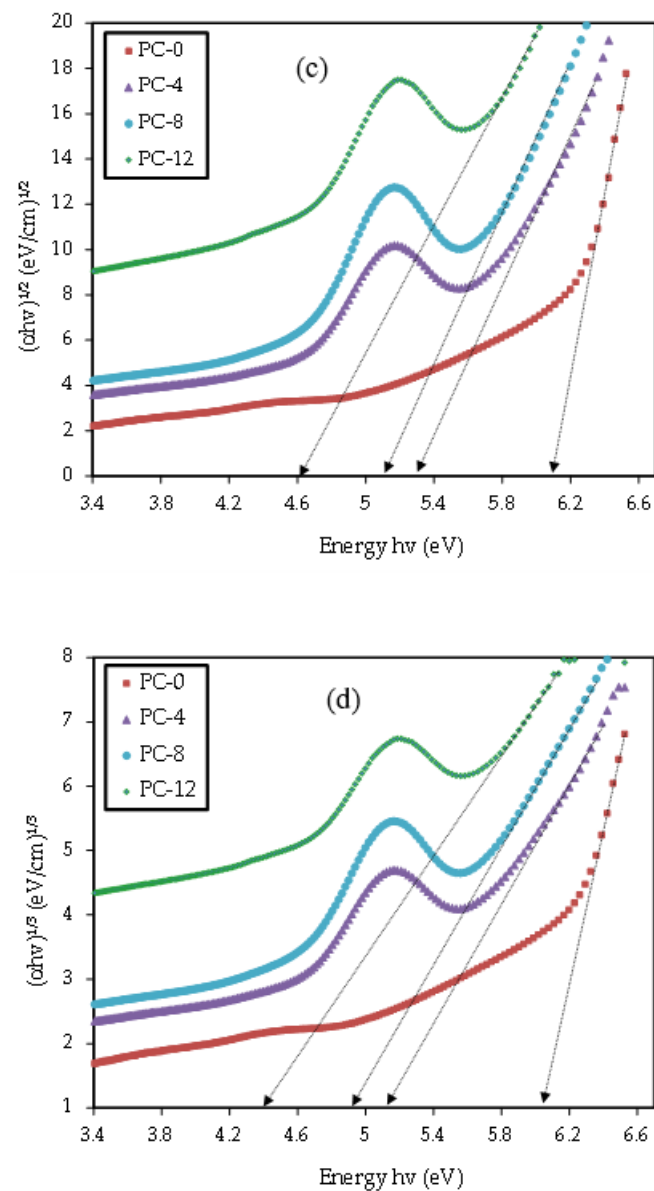


Figure 7. (a) $(\alpha hv)^2$, (b) $(\alpha hv)^{2/3}$, (c) $(\alpha hv)^{1/2}$, and (d) $(\alpha hv)^{1/3}$ versus hv for PVA and doped systems.

Figure 8 shows the kinds of electronic transitions schematically. The intercept of the extrapolated linear components of the figure of $(\alpha hv)^2$ on the x-axis gives the direct optical E_g of both the PVA and PVA composites [45]. Table 3 tabulates the BG values corresponding to all possible transitions. The manipulation of newly formed levels between the valence band (V-B) and conduction band (C-B) of PVA is evidenced by the optical E_g decrease from 6.3 eV for the PVA to 5.25 eV for PVA with 12 wt% of PbS NPs. This reduction also confirms that permanent defects occur at the band edge within the forbidden band. Moreover, it emphasizes that an intermediate energy level will be created in the forbidden gap [46,47]. This is also attributed to the influences of adding PbS NPs, which leads to creating extra electronic states in the PVA BG. Those states serve as intermediate locations for recombination and trapping, causing the optical band gap to modify. The polymer structure change causes an increase in the extent of disordering in the samples and a significant reduction in the E_g [48]. A report published in the literature stated the difficulty of measuring the direct and indirect kinds of amorphous materials [49].

It is clear from Table 3 that the estimated band gap values for composite samples for $\gamma = 3/2$ (direct forbidden) are close enough to those obtained from the optical dielectric loss plot (Figure 9), meaning that the crystalline structure is perturbed in the NCPs samples. Therefore,

the direct forbidden ($\gamma = 3/2$) results for NCPs samples are associated with the reduction of the crystalline order in PVA composite films. The E_g achieved from Tauc’s equation (Figure 7a–d) in comparison to the E_g value obtained from the optical dielectric loss plot (Figure 9) indicates that the nature of electronic transition in pure PVA is direct allowed ($\gamma = 1/2$).

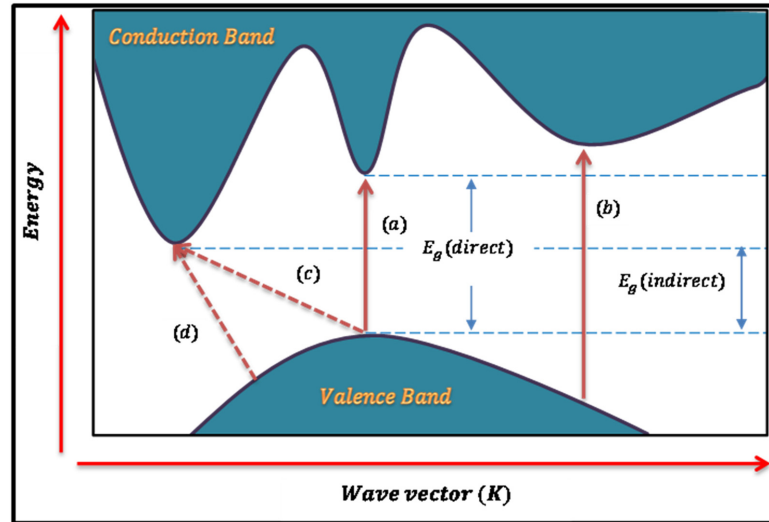


Figure 8. Possible electronic transitions under guiding light through the polymer composite films (a) direct allowed, (b) direct forbidden, (c) indirect allowed, (d) indirect forbidden [21,48].

Table 3. Measured E_g from Tauc and ϵ_i plot.

| Sample Composite | E_g for $\gamma=1/2$ | E_g for $\gamma=3/2$ | E_g for $\gamma=2$ | E_g for $\gamma=1/3$ | Energy Gap from (ϵ_i) eV |
|------------------|------------------------|------------------------|----------------------|------------------------|-------------------------------------|
| PC-0 | 6.34 | 6.19 | 6.11 | 6.05 | 6.3 |
| PC-4 | 5.91 | 5.62 | 5.31 | 5.12 | 5.93 |
| PC-8 | 5.72 | 5.4 | 5.12 | 4.91 | 5.68 |
| PC-12 | 5.4 | 5.02 | 4.61 | 4.41 | 5.25 |

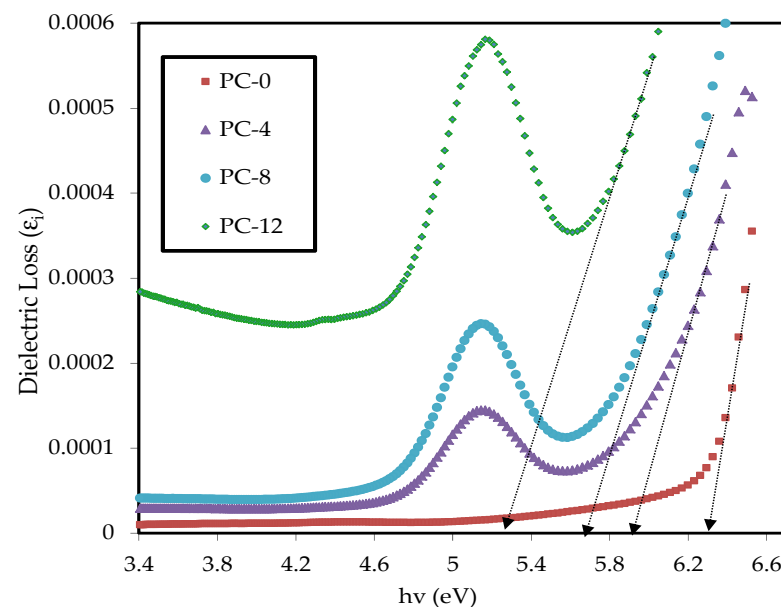


Figure 9. Dielectric losses vs. $h\nu$ for PVA and doped systems.

The current work shows the change in the BG of PVA loaded with PbS NPs and compares with those published for different polymers with several fillers, including ceramics, salts, metal

complexes, and NPs. Table 4 presents how the various filler additions in the previous works did not considerably change the E_g of polymers.

Table 4. E_g associated with various polymer composites in the literature.

| Polymer/Filler Composition | E_g (eV) | References |
|--|-------------|--------------|
| PVA:PbO ₂ | 6.32–4.33 | [13] |
| PVA:CeO ₂ | 6.39–6.18 | [23] |
| PVA:CO ²⁺ metal complex | 6.3–1.6 | [40] |
| PVA:NaNO ₃ | 5.71–5.10 | [50] |
| CS:POZ:Zn ²⁺ -PPL Complex | 4.8–1.6 | [51] |
| PVA:Al ³⁺ metal complex | 6.4–1.81 | [52] |
| PS:SnTiO ₃ | 4.44–3.64 | [53] |
| PEO:CaTiO ₃ | 4.90–4.19 | [54] |
| PS:CaTiO ₃ | 4.42–4.26 | [55] |
| PEO:NaFeF ₄ | 4.54–3.54 | [56] |
| Cs:AgTf:Al ₂ O ₃ | 3.7–3.36 | [57] |
| P(MMA-CO-4VPNO)/KClO ₃ | 3.76–3.65 | [58] |
| PVP/VO ²⁺ | 3.88–3 | [59] |
| PEO/LiCF ₃ So ₃ /DBP/ZrO ₂ | 5.70–5.60 | [60] |
| PVP/Fe ³⁺ | 3.97–3.03 | [61] |
| PMMA /CNDs | 5.03–4.2 | [62] |
| PEO:CNDs:Ag | 6.26–6 | [63] |
| Cs/GO | 3.84–3.80 | [64] |
| PVC/Al ₂ O ₃ | 5.05–3.60 | [65] |
| TiO ₂ -PMMA/FTO | 4.11–3.35 | [66] |
| PEO/ SnTiO ₃ | 5.1–5.0 | [67] |
| Cs/Cu | 5.24–3.72 | [68] |
| PVC/NiO | 5.201–5.150 | [69] |
| PVA:LiI | 5.56–4.95 | [3] |
| PVA:NaI | 5.40–4.90 | [70] |
| PVA:SnBr ₂ | 5.6–3.76 | [12] |
| PVA:NaF | 5.20–4.77 | [71] |
| PVA:CdCl ₂ .H ₂ O | 6.42–5.80 | [72] |
| PVA:NaNO ₃ | 5.6–4.95 | [73] |
| PVA:CuI | 3.39–2.12 | [74] |
| PVA:KMnO ₄ | 6.27–3.12 | [75] |
| PVA:LiAsF ₆ | 5.40–4.87 | [76] |
| PVA:Ba(NO ₃) ₂ | 6.27–4.88 | [42] |
| PVA/ Fullerene C60 | 5.31–4.63 | [77] |
| PVA/g-C ₃ N ₄ | 5.42–3.38 | [78] |
| PVC/fGO | 5.21–5.04 | [79] |
| PVA/GO | 4.09–4.039 | [80] |
| PVA/Fe | 3.5–2.8 | [81] |
| PVA/TiO ₂ | 5.6–2.11 | [82] |
| PVA/PbI ₂ | 5.48–4.88 | [83] |
| PVA/CuO | 6.28–3.18 | [84] |
| PVA/Al | 6.2–5.2 | [48] |
| PVA/BaTiO ₃ | 5.9–5.6 | [30] |
| PVA/Cd _{0.5} Zn _{0.5} Fe ₂ O ₄ | 5.9–2.2 | [15] |
| PVA/HgS | 6.27–4.88 | [28] |
| PVA:Gd ₂ O ₃ :ZnO | 4.90–3.03 | [85] |
| PVA1/Bi | 5.61–5.39 | [86] |
| MC: MB | 6.29–5.95 | [87] |
| PVA: Dy ₂ O ₃ | 5.64–5.23 | [88] |
| PVA:PbS | 3.08–1.97 | [89] |
| PVA:Sulfonamide-vitamin-C | 6.3–3.6 | [90] |
| PEO:Pb ₃ O ₄ | 5.4–1.8 | [91] |
| PVA:Bi ₂ O ₃ Nano Composite | 6.3–3.55 | [92] |
| PVA:PbS Nano Composite | 6.3–5.25 | Present work |

Using the dielectric function from optical spectroscopy is vital to study the overall band structure of materials because of their strong correlation. The earlier study shows that the electron transition from occupied state to unoccupied state is primarily characterized by the imaginary component of the dielectric function (ϵ_i) [93]. However, there is a sophisticated quantum mechanical formulation which can precisely reflect the imaginary component of the dielectric constant [94],

$$\epsilon_{\alpha\beta} = \frac{4\pi^2 e^2}{\Omega m^2 \omega^2} \sum_{k n n' \sigma} f_{n\sigma}^k (1 - f_{n'\sigma}^k) \delta(\xi_{kn'} - \xi_{kn} - \hbar\omega) \times \langle \Psi_{nk\sigma} | P\alpha | \Psi_{n'k\sigma} \rangle \langle \Psi_{n'k\sigma} | P\beta | \Psi_{nk\sigma} \rangle \quad (8)$$

where the functions ($\Psi_{n'k\sigma}$ and $\Psi_{nk\sigma}$) stand for the crystal wave functions from the final and initial states at the k -point. The constant parameters, e , Ω , and m , are the electron charge, volume, and mass, respectively. The $f_{n\sigma}^k$ represents the Fermi energy distribution. In the present study, the optical band gap of the samples was precisely and reliably assessed by applying the idea of optical dielectric loss. In recent years, it has been well established that the absorption edge could be derived from the mutual relationship between dielectric loss and photon energy with comparable outcomes to or almost the same as those obtained from the Tauc's relationship [28,30,42].

Based on the experimental results, a direct calculation of the dielectric function from optical spectroscopy is highly possible. Optical spectroscopy also eases access to crucial parameters such as absorbance, reflectance, refractive index, and extinction coefficient. Therefore, establishing a relationship between the measured parameters and the ϵ_r and ϵ_i is the aim of this work in the attempt to gain a comprehensive understanding of electronic structure within materials that respond to UV-vis radiation. Thus, the easy way of determining the complex dielectric constant from the achieved n and k is the implementation of the below correlation [29]:

$$\epsilon_i = 2nk \quad (9)$$

From Figure 9, one can consider the actual band gap from the intersection of linear components with the x-axis. Nofal et al. [40] have recently concluded that the principal absorption edge comes from the plot associated with dielectric loss versus $h\nu$. The study also emphasized that the absorption edge must be equivalent to or substantially near that calculated from Tauc's theory [40]. Moreover, it will be reasonable to effectively define the interband absorption mechanism from the electron transition between the solid bands. To be clearer, the optical transition onset over the BG is mainly determined by the absorption edge. As mentioned above, the electronic transition types can be measured by comparing the graphs from Tauc's method (see Figure 7a–d) to Figure 9. From those figures, it was concluded that PVA's electronic transition type is directly allowed, whereas PVA:PbS samples are directly forbidden. Eventually, from the previous findings, the band gap structure and the dielectric function can be analyzed [63].

The long wavelength range and low frequency (ν) are strongly correlated. This results in photons with low energy ($E = h\nu$), making it impossible for them to move electrons from the V-B to the C-B. So, electrons lose energy by scattering. The optical characteristics of materials are described from the index of refraction and the dielectric constant. A clear relationship is seen in Equation (10), where n and K values can also be derived from ϵ_r .

$$\epsilon_r = n^2 - k^2 \quad (10)$$

Figure 10 shows the essential interrelationship between the ϵ_r and λ for the samples. Based on the Spitzer–Fan model, the wavelength and refractive index relationship were used to obtain the dielectric response at high frequency (short wavelengths) [95]:

$$\epsilon_r = n^2 - k^2 = \epsilon_\infty - \left(\frac{e^2}{4\pi^2 c^2 \epsilon_0} \right) \times \left(\frac{N}{m^*} \right) \lambda^2 \quad (11)$$

where ϵ_0 , c , and N are the permittivity of vacuum, speed of light, and the amount of charge carrier per unit volume, respectively. m^* stands for the effective mass, which is $1.16 m_e$ [52].

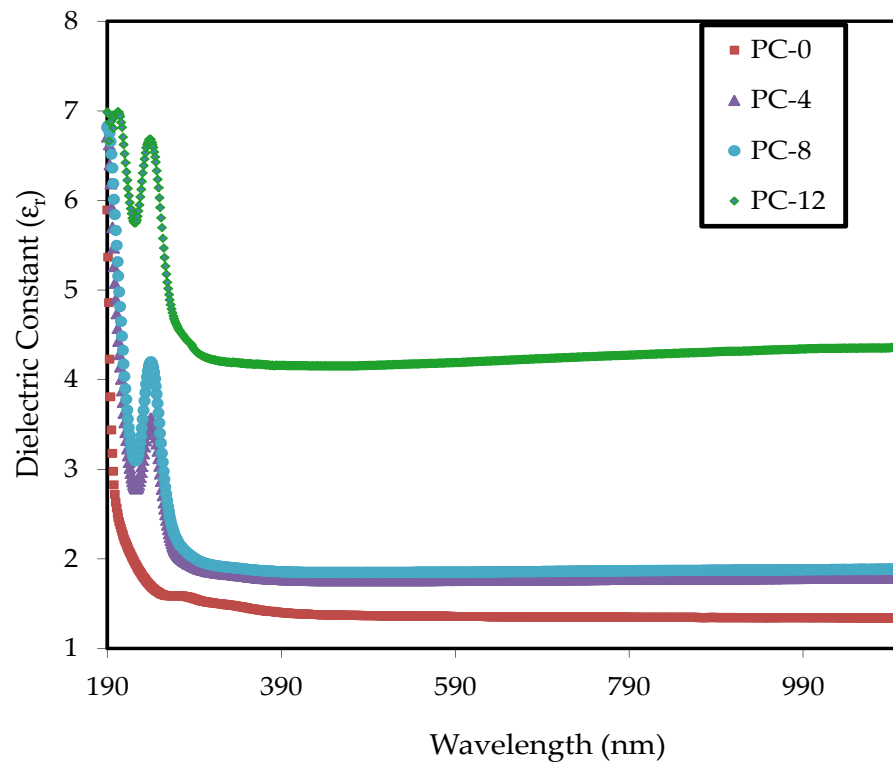


Figure 10. ϵ_r for PVA and PVA-loaded samples.

Here, the dielectric constant in its complex form is equivalent to the complex refractive index square ($n = \epsilon_r^{1/2}$). Additionally, it indicates how much the material can decrease the speed of light [48]. Figure 11 shows the relationship between the ϵ_r and λ^2 in the visible range. The slope value and intercept with the y-axis can be applied to determine the N/m^* and ϵ_∞ values, respectively. The estimation of the values of ϵ_∞ , N/m^* , and N were obtained from Equation (11).

Table 5 shows that the magnitudes of charge carriers (N/m^*) in pure PVA increased as the filler concentration increased from 3.65×10^{55} to $281.02 \times 10^{55} \text{ m}^3/\text{Kg}$. Furthermore, the ϵ_∞ increased from 1.37 to 4.44, indicating a rise in free charge carriers that effectively contributed to the polarization process [52].

There is a connection between the CDF and the assessable optical values using simple equations, from which a rough computation of the optical properties of solids can be performed. The ϵ_r and ϵ_i and the density of newly induced localized states of electrons within the forbidden band gap have experienced behavior that is robustly in accordance with prior studies. Upon using (N/m^*) values, the prediction of many other crucial parameters from the Drude free electron model is possible, such as relaxation time (τ), plasma frequency (ω_p), and electrical resistivity (ρ) [40]:

$$\epsilon_i = J \left(\frac{1}{\tau} \right) \lambda^3, \quad J = \frac{e^2}{8\pi^3 C^3 \epsilon_0} \frac{N}{m^*} \tag{12}$$

Figure 12 shows the variation of ϵ_i with respect to λ^3 for a pure PVA and the other films with various quantities of PbS NPs in the region where linear behavior is obtainable. The relaxation time (τ) values would be derived from Equation (12) using the N/m^* value

and the slope of linear correlation of ϵ_i versus λ^3 . Moreover, to calculate the optical mobility (μ_{opt}), ρ_{opt} , and ω_p of the electron, the following relationships can be applied [40]:

$$\mu_{opt} = \frac{e\tau}{m^*} \tag{13}$$

$$\rho_{opt} = \frac{1}{e\mu_{opt}N_c} \tag{14}$$

$$\omega_p = \frac{e^2N}{\epsilon_0 m^*} \tag{15}$$

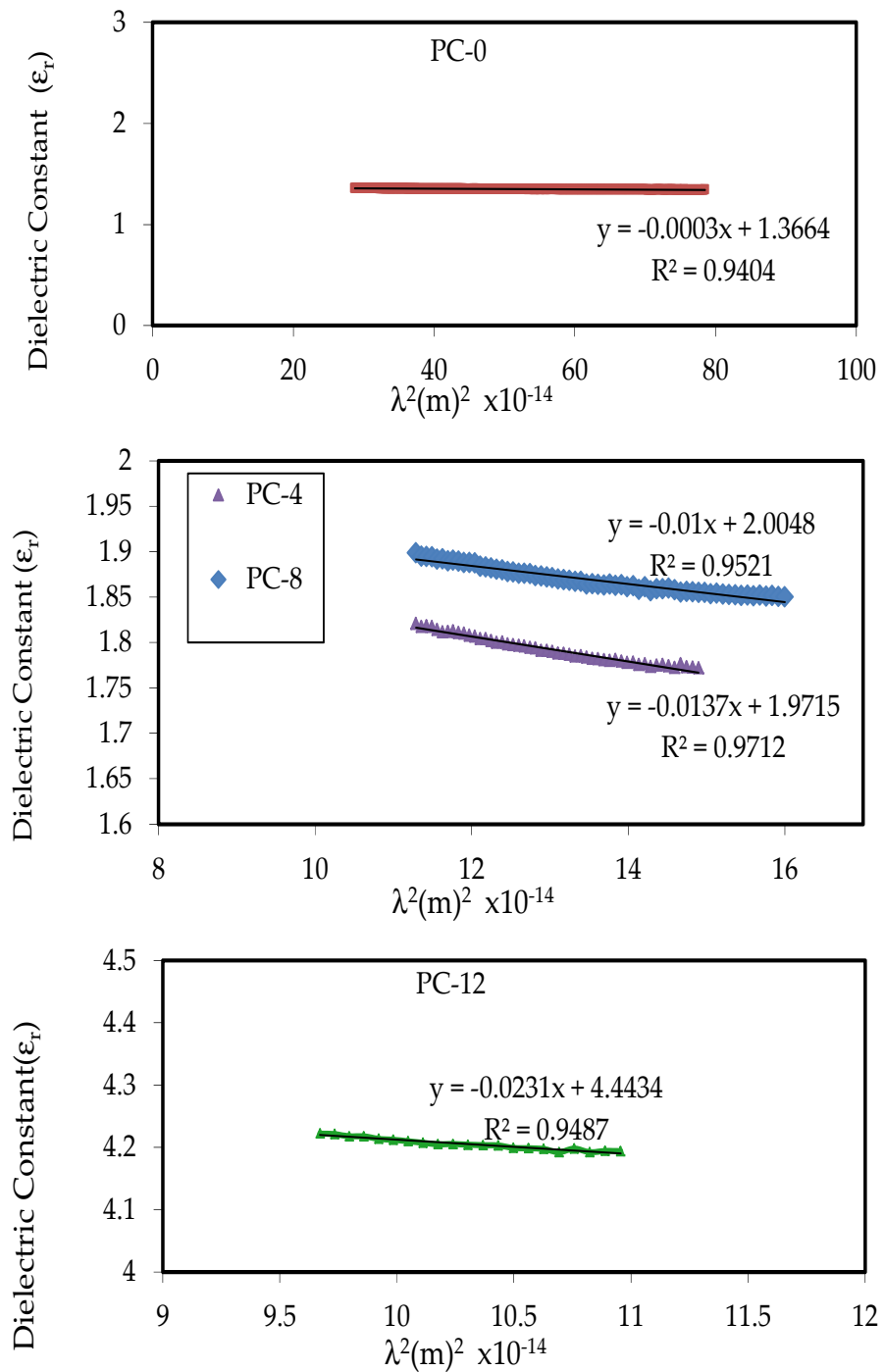


Figure 11. Linear plots of ϵ_r versus λ^2 .

Table 5. Optical dielectric parameters associated with pure PVA and PVA containing PbS.

| Sample Composite | $N/m^* \times 10^{55} \text{ m}^3/\text{kg}$ | ϵ_∞ |
|------------------|--|-------------------|
| PC-0 | 3.65 | 1.37 |
| PC-4 | 166.67 | 1.97 |
| PC-8 | 121.66 | 2.01 |
| PC-12 | 281.02 | 4.44 |

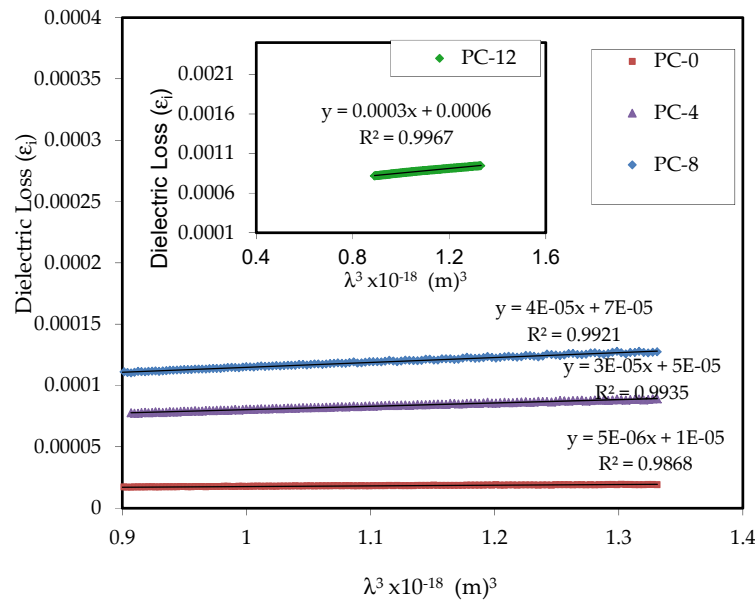


Figure 12. Plots of ϵ_i versus λ^3 for the systems.

Table 6 shows the values of τ and ω_p . It is worth mentioning that the τ , μ_{opt} , and ρ_{opt} of PVA are manipulated in a lower trend upon the addition of PbS NOF. This incorporation of the filler leads to a much faster relaxation response of the NCP molecules to the guided electromagnetic field than the unfilled one.

Table 6. Determined values of τ , μ_{opt} , ρ_{opt} , and ω_p .

| Sample Composite | τ (fs) | μ (opt) | $N_c \times 10^{25}$ | $\rho(opt) \times 10^{-8}$ | $\omega_p \times 10^{29}$ |
|------------------|-------------|-------------|----------------------|----------------------------|---------------------------|
| PC-0 | 3.2 | 4.85 | 3.86 | 50.5 | 1.06 |
| PC-4 | 24.3 | 36.9 | 176 | 0.145 | 48.3 |
| PC-8 | 13.3 | 20.2 | 129 | 0.363 | 35.3 |
| PC-12 | 4.1 | 6.22 | 297 | 0.511 | 81.5 |

The low values of τ , μ_{opt} and ρ_{opt} are a result of slowing down the light beam through polymer material films with relatively larger refractive indices. The ω_p of the electron increased from 1.06×10^{29} to 81.5×10^{29} Hz when the PbS NPs was added. A comparable outcome collected for NCPs and the effect of an intensive local electric field of induced NOF dipole moment has been reported. This enhances the material’s polarization whenever exposed to the external electromagnetic field. The calculation of optical parameters can also be carried out. The previous explanation indicates that there is more than one way to evaluate the E_g such as using refractive index and the optical dielectric loss function. These factors are outstanding and decisive in choosing appropriate materials for optoelectronic applications [40].

3.2.4. Refractive Index Study

Figure 13 shows the refractive index (n) and wavelength correlation of PVA and loaded films. It is noticeable that the refractive index increases with the increase of PbS NPs.

Recently, it has been observed that the demand for suitable optical materials with efficient n has increased, particularly in a wide range of optical applications, such as ophthalmic lenses, optical adhesives, lenses, optoelectronics, filters, highly reflecting, and antireflecting coatings [48,84]. As seen in Figure 13, the addition of PbS NPs increased the value of n of the NCPs samples. Quantitatively, the n values are increased from 1.27 to around 2.16. Lü et al. [96] described how adding some semiconductor NPs of metal sulfide, such as PbS, which have a high refractive index, into a polymer matrix, fabricates NCPs with a high refractive index.

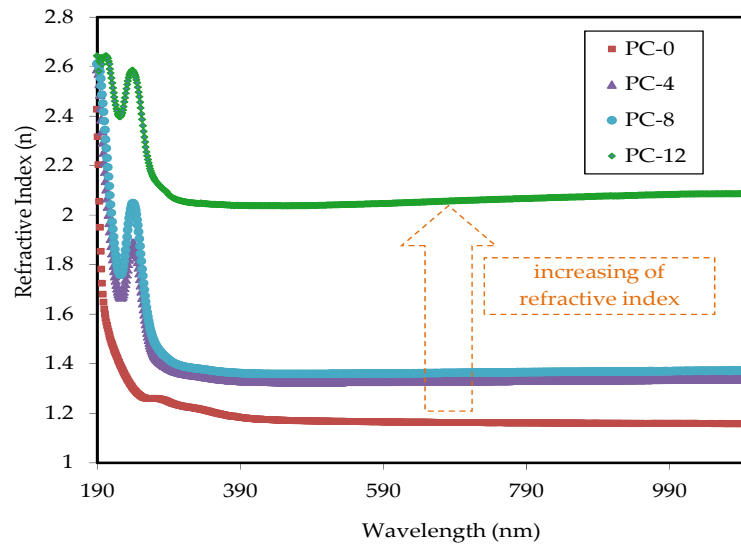


Figure 13. n variation as a function of wavelength.

The extinction coefficient (K) and wavelength relationship are shown in Figure 14. By applying Kramers–Kronig relationships, the n values are obtained from R and K [52]:

$$n = \frac{1 + R}{1 - R} + \sqrt{\frac{4R}{(1 - R)^2} - K^2} \tag{16}$$

where $K = \alpha \times \frac{\lambda}{4\pi t}$.

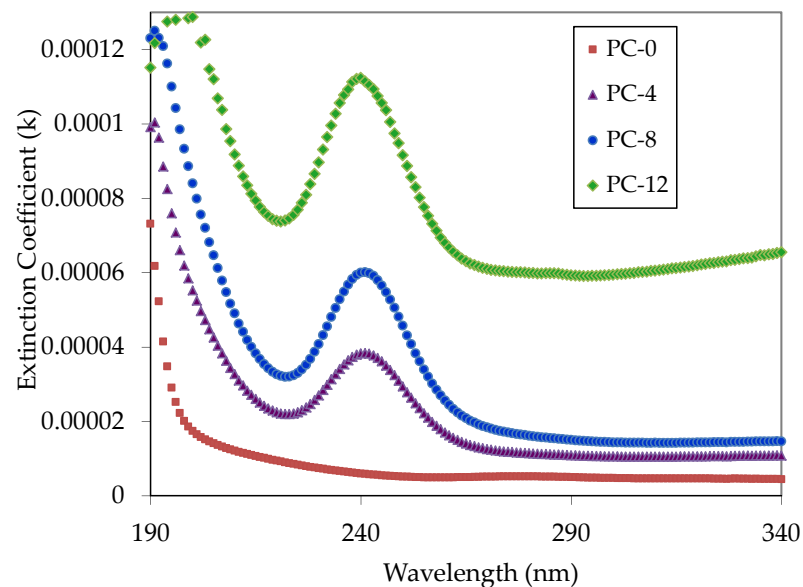


Figure 14. Extinction coefficients (k) over a broad wavelength range.

The k has a high value for the loaded samples at longer wavelengths. The k determines the amount of light loss because of absorption and scattering per unit distance of the guiding medium. The magnitude of (k) shows the degree of transparency of the films at the long wavelengths [48].

On the other hand, at short wavelengths the k obtains the maximum value immediately because the absorption behavior predominates. Figure 14 shows that k increases when the PbS NPs quantity in PVA films increases. When the material under study is subjected to electromagnetic radiation, the composite films dissipate higher energy than those made that of pure PVA, according to the higher k value [73].

3.2.5. Wemple–DiDomenico (WD) Model

It is crucial to determine the refractive index and the dispersion behavior as two essential optical properties of materials. For optical communication and the development of the device, the determination of the refractive index dispersion and spectral dispersion is essential. Regarding the normal dispersion region, the n is thoroughly studied using the single oscillator model proposed by WD. Dispersion energy (E_d) represents a direct measurement of the strength of the inter-band optical transition. The E_d also identifies a strong connection to the chemical bonding and combines the charge distribution and coordination number in each unit cell. A single oscillator parameter (E_o) is directly proportional to the oscillator’s energy. The following semi-empirical relationship can be used in the correlation between the refractive index and photon energy [40]:

$$(n^2 - 1)^{-1} = \frac{E_o}{E_d} - \left(\frac{1}{E_d E_o} \right) (hv)^2 \tag{17}$$

The magnitudes of both E_d and E_o from the intercept and slope, respectively, can be determined. The data in Figure 15 were fitted using linear regression lines. The calculated E_o and E_d are tabulated in Table 7. The E_d values increased with increasing PbS NPs values, while E_o values decreased. E_o and the optical E_g are interrelated. Empirically, the E_o values reflect the direct E_g (i.e., $E_o \approx E_g$) for the obtained films, as shown in Table 3 [23,40]. The slope of the linear section of $(n^2 - 1)^{-1}$ verses $(hv)^2$ produces the $\left(\frac{1}{E_d E_o} \right)$ values. Figure 15 shows that the intersection of the graph and the y-axis yields the $\frac{E_o}{E_d}$ values [40].

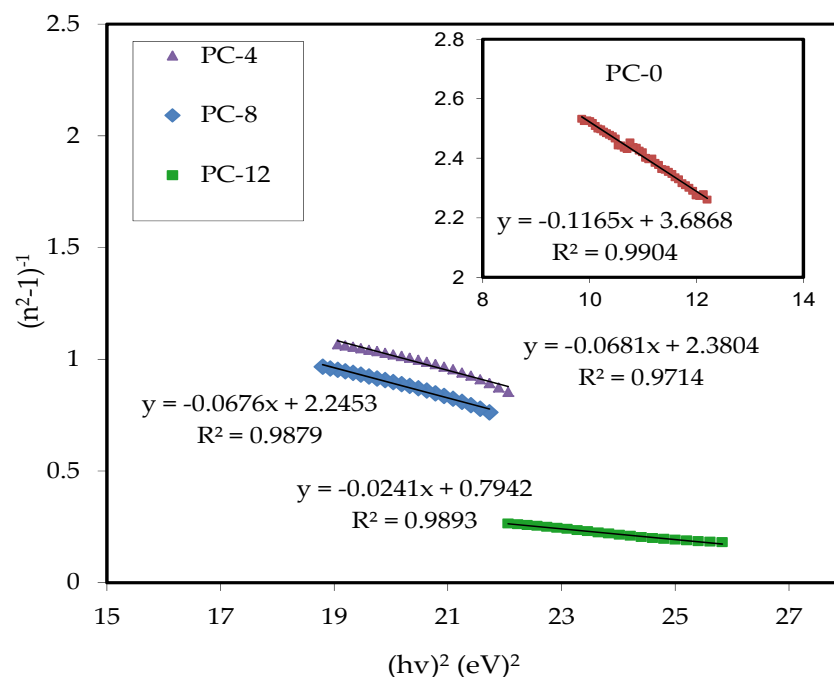


Figure 15. Variation of $(n^2 - 1)^{-1}$ against photon energy $(hv)^2$ for the samples.

Table 7. Optical band gap calculated from the single oscillator model, established by Wemple–DiDomenico.

| Sample Composite | E_d | E_o | n^o |
|------------------|-------|-------|-------|
| PC-0 | 1.53 | 5.63 | 1.27 |
| PC-4 | 2.48 | 5.91 | 1.42 |
| PC-8 | 2.57 | 5.76 | 1.45 |
| PC-12 | 7.23 | 5.74 | 2.26 |

4. Conclusions

In conclusion, it is suitable to synthesis the PVA/PbS polymer NCPs film using the solution cast method. The PbS NPs primarily decreased the degree of crystallinity of the polymer NCPs. The FTIR outcome showed the occurrence of interaction among polymer NCPs components. The strong absorption of NCPs films in the UV region showed the suitability of the films for UV shielding. In addition, the PbS NPs content within the PVA matrix decreased the E_g value from 6.3 to 5.25 eV. Furthermore, the magnitude of E_U increased from 0.20 to 1.30 eV upon loading PbS NPs into the polymer, indicating the occurrence of structural disordering in polymers and leading to an increase in locally induced new states in the forbidden gaps. From the optics point of view, the refractive index improved from 1.27 to 2.16, corresponding to the polymer composite film with optimum PbS NPs. From the optical dielectric loss plot, the exact values of E_g were determined and used to specify the types of electron transition proposed from the Tauc's model for each solid film. The ω_p of the electron increased from 1.06×10^{29} to 81.5×10^{29} Hz when the PbSNPs was added. The μ of the electron also increased from 4.85 to 6.22 $\text{cm}^2/(\text{V}\cdot\text{s})$ by adding the PbS NPs. Owing to their optical band gap, enhanced optical property and flexibility, these samples have a good potential for application in optoelectronic devices.

Author Contributions: Conceptualization, S.M.M., S.A.H. and S.B.A.; Data curation, P.A.M.; Formal analysis, S.A.H.; Investigation, A.H.A.D.; Methodology, A.H.A.D.; Project administration, S.A.H. and S.B.A.; Supervision, S.A.H. and S.B.A.; Validation, P.A.M., S.M.M., S.B.A., M.A.B., R.M.A. and W.O.K.; Writing—original draft, A.H.A.D. and P.A.M.; Writing—review and editing, S.M.M., S.B.A., M.A.B., R.M.A. and W.O.K. All authors have read and agreed to the published version of the manuscript.

Funding: The authors gratefully acknowledge the financial support for this study from the Ministry of Higher Education and Scientific Research, Kurdistan Regional Government, Department of Physics, College of Science, University of Sulaimani, Sulaimani.

Institutional Review Board Statement: Not applicable.

Informed Consent Statement: Not applicable.

Data Availability Statement: Not applicable.

Conflicts of Interest: The authors declare no conflict of interest.

References

- Chang, C.; Chang, C. Preparation and characterization of polyimide e nanogold nanocomposites from 3-mercaptopropyltrimethoxysilane encapsulated gold nanoparticles. *Polym. Degrad. Stab.* **2008**, *93*, 109–116. [[CrossRef](#)]
- Clark, J.; Lanzani, G. Organic photonics for communications. *Nat. Photonics* **2010**, *4*, 438–446. [[CrossRef](#)]
- Ahmad, H.M.; Sabeeh, S.H.; Hussen, S.A. Electrical and Optical Properties of PVA/LiI Polymer Electrolyte Films. *Asian Trans. Sci. Technol.* **2012**, *1*, 16–20.
- Cardona, D.M.M.; Florez, J.J.O. Electrical properties of Cr/CrN nano-multilayers produced by the unbalanced magnetron sputtering technique. *Dyna* **2011**, *78*, 53–57.
- Mamiyev, Z.; Balayeva, N.O. PbS nanostructures: A review of recent advances, Materials Today Sustainability. *Mater. Today Sustain.* **2023**, *21*, 100305. [[CrossRef](#)]
- Melnikov, P.; Bobrov, A.; Marfin, Y. On the Use of Polymer-Based Composites for the Creation of Optical Sensors: A Review. *Polymers* **2022**, *14*, 4448. [[CrossRef](#)]
- John, B. Polymer Nanocomposite-Based Electrochemical Sensors and Biosensors. In *Nanorods Nanocomposites*; IntechOpen: London, UK, 2020. [[CrossRef](#)]

8. Brza, M.A.; Aziz, S.B.; Anuar, H.; Al Hazza, M.H.F. From green remediation to polymer hybrid fabrication with improved optical band gaps. *Int. J. Mol. Sci.* **2019**, *20*, 3910. [[CrossRef](#)] [[PubMed](#)]
9. Brza, M.A.; Aziz, S.B.; Anuar, H.; Ali, F.; Dannoun, E.; Mohammed, S.J.; Abdulwahid, R.T.; Al-Zangana, S. Tea from the drinking to the synthesis of metal complexes and fabrication of PVA based polymer composites with controlled optical band gap. *Sci. Rep.* **2020**, *10*, 18108. [[CrossRef](#)]
10. Abdullah, O.G.; Salman, Y.A.K.; Saleem, S.A. Electrical conductivity and dielectric characteristics of in situ prepared PVA/HgS nanocomposite films. *J. Mater. Sci. Mater. Electron.* **2016**, *27*, 3591–3598. [[CrossRef](#)]
11. Abdullah, O.G.H.; Saleem, S.A. Effect of Copper Sulfide Nanoparticles on the Optical and Electrical Behavior of Poly (vinyl alcohol) Films. *J. Electron. Mater.* **2016**, *45*, 5910–5920. [[CrossRef](#)]
12. Khairy, Y.; Mohammed, M.I.; Elsaedy, H.I.; Yahia, I.S. Optical and electrical properties of SnBr₂-doped polyvinyl alcohol (PVA) polymeric solid electrolyte for electronic and optoelectronic applications. *Opt. Int. J. Light Electron. Opt.* **2020**, *228*, 166129. [[CrossRef](#)]
13. Abdulwahid, R.T.; Abdullah, O.G.; Aziz, S.B.; Hussein, S.A.; Muhammad, F.F.; Yahya, M.Y. The study of structural and optical properties of PVA: PbO₂ based solid polymer nanocomposites. *J. Mater. Sci. Mater. Electron.* **2016**, *27*, 12112–12118. [[CrossRef](#)]
14. Badawi, A. Engineering the optical properties of PVA/PVP polymeric blend in situ using tin sulfide for optoelectronics. *Appl. Phys. A* **2020**, *126*, 335. [[CrossRef](#)]
15. Soliman, T.S.; Abouhaswa, A.S. Synthesis and structural of Cd_{0.5}Zn_{0.5}F₂O₄ nanoparticles and its influence on the structure and optical properties of polyvinyl alcohol films. *J. Mater. Sci. Mater. Electron.* **2020**, *31*, 9666–9674. [[CrossRef](#)]
16. Bhajantri, J.N.R.F. Physical and Electrochemical Studies on Ceria Filled PVA Proton Conducting Polymer Electrolyte for Energy Storage Applications. *J. Inorg. Organomet. Polym. Mater.* **2018**, *28*, 906–919. [[CrossRef](#)]
17. Drishya, V.; Unnimaya, A.N.; Naveenraj, R.; Suresh, E.K.; Ratheesh, R. Preparation, Characterization, and Dielectric Properties of PP/CaTiO₃ Composites for Microwave Substrate Applications. *Int. J. Appl. Ceram. Technol.* **2016**, *13*, 810–815. [[CrossRef](#)]
18. Mazzapioda, L.; Vecchio, C.L.; Danyliv, O.; Baglio, V. Composite Nafion-CaTiO₃- δ Membranes as Electrolyte Component for PEM Fuel Cells. *Polymers* **2020**, *12*, 2019. [[CrossRef](#)]
19. Kumar, A.; Kumar, S.; Bahuguna, A.; Kumar, A.; Sharma, V.; Krishnan, V. Recyclable, bifunctional composites of perovskite type N-CaTiO₃ and reduced graphene oxide as an efficient adsorptive photocatalyst for environmental remediation. *Mater. Chem. Front.* **2017**, *1*, 2391–2404. [[CrossRef](#)]
20. Alvarez-Sanchez, C.O.; Lasalde-Ramírez, J.A.; Ortiz-Quiles, E.O.; Massó-Ferret, R.; Nicolau, E. Polymer-MTiO₃ (M = Ca, Sr, Ba) composites as facile and scalable supercapacitor separators. *Energy Sci. Eng.* **2019**, *7*, 730–740. [[CrossRef](#)]
21. Parveen, A.; Koppalkar, A.R.; Roy, A.S. Surface modified CaTiO₃ loaded in polyaniline by sodium dodecyl benzene sulphonic acid for humidity sensor. *IEEE Sens. J.* **2012**, *12*, 2817–2823. [[CrossRef](#)]
22. Mohamad, A.H.; Abdullah, O.G.; Saeed, S.R. Effect of very fine nanoparticle and temperature on the electric and dielectric properties of MC-PbS polymer nanocomposite films. *Results Phys.* **2019**, *16*, 102898. [[CrossRef](#)]
23. Aziz, S.B.; Dannoun, E.M.A.; Tahir, D.A.; Hussen, S.A.; Abdulwahid, R.T.; Nofal, M.M.; Abdullah, R.M.; Hussein, A.M.; Brevik, I. Synthesis of PVA/CeO₂ based nanocomposites with tuned refractive index and reduced absorption edge: Structural and optical studies. *Materials* **2021**, *14*, 1570. [[CrossRef](#)] [[PubMed](#)]
24. Kord, M.; Hedayati, K.; Farhadi, M. Green synthesis and characterization of flower-like PbS and metal-doped nanostructures via hydrothermal method. *Main Group Met. Chem.* **2017**, *40*, 35–40. [[CrossRef](#)]
25. Adeyemi, J.O.; Onwudiwe, D.C. PbS Nanoparticles Prepared Using 1, 10-Phenanthroline Adduct of Lead(II) Bis(N-alkyl-N-phenyl dithiocarbamate) as Single Source Precursors. *Molecules* **2020**, *25*, 2097. [[CrossRef](#)]
26. Sarkawt A Hussen, Structural and optical characterization of pure and SnZrO₃ doped PS based polymer nanocomposite. *Mater. Res. Express* **2020**, *7*, 105302. [[CrossRef](#)]
27. Bhargav, P.B.; Mohan, V.M.; Sharma, A.K.; Rao, V.V.R.N. Investigations on electrical properties of (PVA:NaF) polymer electrolytes for electrochemical cell applications. *Curr. Appl. Phys.* **2009**, *9*, 165–171. [[CrossRef](#)]
28. Abdullah, O.G.; Salman, Y.A.K.; Saleem, S.A. In-situ Synthesis of PVA/HgS Nanocomposite Films and Tuning Optical Properties. *Phys. Mater. Chem.* **2015**, *3*, 18–24. [[CrossRef](#)]
29. Parveen, A.; Agrawal, S.; Azam, A. Band gap tuning and fluorescence properties of lead sulfide Pb_{0.9}A_{0.1}S (A:Fe, Co and Ni) nanoparticles by transition metal doping. *Opt. Mater.* **2018**, *76*, 20–27. [[CrossRef](#)]
30. Soliman, T.S.; Zaki, M.F.; Hessien, M.M.; Elkalashy, S.I. The structure and optical properties of PVA-BaTiO₃ nanocomposite films. *Opt. Mater.* **2020**, *111*, 110648. [[CrossRef](#)]
31. Aziz, S.B.; Brza, M.A.; Nofal, M.M.; Abdulwahid, R.T.; Hussen, S.A.; Hussein, A.M.; Karim, W.O. A comprehensive review on optical properties of polymer electrolytes and composites. *Materials* **2020**, *13*, 3675. [[CrossRef](#)] [[PubMed](#)]
32. Hemalatha, K.S.; Rukmani, K.; Suriyamurthy, N.; Nagabhushana, B.M. Synthesis, characterization and optical properties of hybrid PVA-ZnO nanocomposite: A composition dependent study. *Mater. Res. Bull.* **2014**, *51*, 438–446. [[CrossRef](#)]
33. Kumar, R.; Ali, S.A.; Mahur, A.K.; Virk, H.S.; Singh, F.; Khan, S.A.; Avasthi, D.K.; Prasad, R. Study of optical band gap and carbonaceous clusters in swift heavy ion irradiated polymers with UV-Vis spectroscopy. *Nucl. Instrum. Methods Phys. Res. Sect. B Beam Interact. Mater. At.* **2008**, *266*, 1788–1792. [[CrossRef](#)]
34. Ennis, C.P.; Kaiser, R.I. Mechanistical studies on the electron-induced degradation of polymethylmethacrylate and Kapton. *Phys. Chem. Chem. Phys.* **2010**, *12*, 14902–14915. [[CrossRef](#)]

35. Maikala, R.V. Modified Beer's Law—Historical perspectives and relevance in near-infrared monitoring of optical properties of human tissue. *Int. J. Ind. Ergon.* **2010**, *40*, 125–134. [[CrossRef](#)]
36. Kuntzleman, T.S.; Jacobson, E.C. Teaching Beer's Law and absorption spectrophotometry with a smart phone: A substantially simplified protocol. *J. Chem. Educ.* **2016**, *93*, 1249–1252. [[CrossRef](#)]
37. Aziz, S.B.; Hassan, A.Q.; Mohammed, S.J.; Karim, W.O.; Kadir, M.F.Z.; Tajuddin, H.A.; Chan, N.N.M.Y. Structural and optical characteristics of pva:C-dot composites: Tuning the absorption of ultra violet (uv) region. *Nanomaterials* **2019**, *9*, 216. [[CrossRef](#)]
38. Aziz, S.B.; Gh, O.; Ahang, A. Optical properties of pure and doped PVA: PEO based solid polymer blend electrolytes: Two methods for band gap study. *J. Mater. Sci. Mater. Electron.* **2017**, *28*, 7473–7479. [[CrossRef](#)]
39. Guirguis, O.W.; Moselhey, M.T.H. Optical study of poly(vinyl alcohol)/hydroxypropyl methylcellulose blends. *J. Mater. Sci.* **2011**, *46*, 5775–5789. [[CrossRef](#)]
40. Nofal, M.M.; Aziz, S.B.; Hadi, J.M.; Karim, W.O.; Dannoun, E.M.A.; Hussein, A.M.; Hussen, S.A. Polymer composites with 0.98 transparencies and small optical energy band gap using a promising green methodology: Structural and optical properties. *Polymers* **2021**, *13*, 1648. [[CrossRef](#)]
41. Aziz, S.B.; Rasheed, M.A.; Hussein, A.M.; Ahmed, H.M. Fabrication of polymer blend composites based on [PVA-PVP]_(1-x):(Ag₂S)_x (0.01 ≤ x ≤ 0.03) with small optical band gaps: Structural and optical properties. *Mater. Sci. Semicond. Process.* **2017**, *71*, 197–203. [[CrossRef](#)]
42. Abdullah, O.G.; Prof, A. Influence of barium salt on optical behavior of pva based solid polymer. *Eur. Sci. J.* **2014**, *10*, 406–417.
43. Krishnakumar, V.; Govindaraj, S. Electrical and optical properties of pure and Pb²⁺ ion doped PVA—PEG polymer composite electrolyte films. *Ionics* **2011**, *18*, 403–411. [[CrossRef](#)]
44. Abdullah, O.G.; Aziz, S.B.; Rasheed, M.A. Incorporation of NH₄ NO₃ into MC-PVA blend-based polymer to prepare proton-conducting polymer electrolyte films. *Ionics* **2017**, *24*, 777–785. [[CrossRef](#)]
45. Abdelhamied, M.M.; Atta, A. Synthesis and Optical Properties of PVA/PANI/Ag Nanocomposite films. *J. Mater. Sci. Mater. Electron.* **2020**, *31*, 22629–22641. [[CrossRef](#)]
46. Patel, G.B.; Singh, N.L.; Singh, F. Modification of chitosan-based biodegradable polymer by irradiation with MeV ions for electrolyte applications. *Mater. Sci. Eng. B Solid-State Mater. Adv. Technol.* **2017**, *225*, 150–159. [[CrossRef](#)]
47. Lee, E.H. Ion-beam modification of polymeric materials—Fundamental principles and applications. *Nucl. Instrum. Methods Phys. Res. Sect. B Beam Interact. Mater. At.* **1999**, *151*, 29–41. [[CrossRef](#)]
48. Aziz, S.B.; Ahmed, H.M.; Hussein, A.M.; Fathulla, A.B.; Wsw, R.M.; Hussein, R.T. Tuning the absorption of ultraviolet spectra and optical parameters of aluminum doped PVA based solid polymer composites. *J. Mater. Sci. Mater. Electron.* **2015**, *26*, 8022–8028. [[CrossRef](#)]
49. Rodríguez, A.; Sánchez Vergara, M.E.; García Montalvo, V.; Ortiz, A.; Alvarez, J.R. Thin films of molecular materials synthesized from C₃₂H₂₀N₁₀M (M = Co, Pb, Fe): Film formation, electrical and optical properties. *Appl. Surf. Sci.* **2010**, *256*, 3374–3379. [[CrossRef](#)]
50. Muhammadsharif, F.F.; Aziz, S.B.; Hussen, S. Effect of the dopant salt on the optical parameters of PVA: NaNO₃ solid polymer electrolyte Effect of the dopant salt on the optical parameters of PVA: NaNO₃ solid polymer electrolyte. *J. Mater. Sci. Mater. Electron.* **2014**, *26*, 521–529. [[CrossRef](#)]
51. Khayal, K.; Ahmeda, A.; Hussena, S.; Azizab, S.B. Transferring the wide band gap chitosan: POZ-based polymer blends to small optical energy band gap polymer composites through the inclusion of green synthesized Zn²⁺-PPL metal complex. *Arab. J. Chem.* **2022**, *15*, 103913. [[CrossRef](#)]
52. Aziz, S.B.; Nofal, M.M.; Ghareeb, H.O.; Dannoun, E.M.A.; Hussen, S.A.; Hadi, J.M.; Ahmed, K.K.; Hussein, A.M. Characteristics of poly(Vinyl alcohol) (PVA) based composites integrated with green synthesized Al³⁺-metal complex: Structural, optical, and localized density of state analysis. *Polymers* **2021**, *13*, 1316. [[CrossRef](#)] [[PubMed](#)]
53. Hussein, A.M.; Dannoun, E.M.A.; Aziz, S.B.; Brza, M.A.; Abdulwahid, R.T.; Hussen, S.A.; Rostam, S.; Mustafa, D.M.T.; Muhammad, D.S. Steps toward the band gap identification in polystyrene based solid polymer nanocomposites integrated with tin titanate nanoparticles. *Polymers* **2020**, *12*, 2320. [[CrossRef](#)] [[PubMed](#)]
54. Aziz, S.B.; Nofal, M.M.; Brza, M.A.; Hussein, S.A.; Mahmoud, H.; El-bahy, Z.M.; Dannoun, E.M.A.; Kareem, W.O.; Hussein, A.M. Characteristics of PEO Incorporated with CaTiO₃ Nanoparticles: Structural and Optical Properties. *Polymers* **2021**, *13*, 3484. [[CrossRef](#)]
55. Ezat, G.S.; Hussen, S.A.; Aziz, S.B. Structure and optical properties of nanocomposites based on polystyrene (PS) and calcium titanate (CaTiO₃) perovskite nanoparticles. *Optik* **2021**, *241*, 166963. [[CrossRef](#)]
56. Taylor, P.; Mohan, V.M.; Bhargav, P.B.; Raja, V.; Sharma, A.K. Optical and Electrical Properties of Pure and Doped PEO Polymer Electrolyte Films. *Soft Mater.* **2007**, *5*, 33–46. [[CrossRef](#)]
57. Aziz, S.B.; Mamand, S.M.; Saed, S.R.; Abdullah, R.M.; Hussein, S.A. New Method for the Development of Plasmonic Metal-Semiconductor Interface Layer: Polymer Composites with Reduced Energy Band Gap. *J. Nanomater.* **2017**, *2017*, 7459218. [[CrossRef](#)]
58. Raja, V.; Mohan, V.M.; Sharma, A.K. Electrical and optical properties of pure and KClO₃ -doped P (MMA-CO-4VPNO) polymer electrolyte films. *Ionics* **2009**, *15*, 519–524. [[CrossRef](#)]
59. Sreekanth, K.; Siddaiah, T.; Gopal, N.O.; Kumar, Y.M.; Ramu, C. Optical and electrical conductivity studies of VO²⁺ doped polyvinyl pyrrolidone (PVP) polymer electrolytes. *J. Sci. Adv. Mater. Devices* **2019**, *4*, 230–236. [[CrossRef](#)]

60. Mariah, S.; Yasin, M.; Ibrahim, S.; Johan, M.R. Effect of Zirconium Oxide Nanofiller and Dibutyl Phthalate Plasticizer on Ionic Conductivity and Optical Properties of Solid Polymer Electrolyte. *Sci. World J.* **2014**, *2014*, 547076. [[CrossRef](#)]
61. Sreekanth, K.; Siddaiah, T.; Gopal, N.O.; Kumar, Y.M.; Ramu, C.; Siddaiah, T.; Gopal, N.O.; Kumar, Y.M.; Ramu, C. Thermal, structural, optical and electrical conductivity studies of pure and Fe ions doped PVP films for semiconducting polymer devices. *Mater. Res. Innov.* **2020**, *25*, 95–103. [[CrossRef](#)]
62. Aziz, S.B.; Abdullah, O.G.; Brza, M.A.; Azawy, A.K.; Tahir, D.A. Effect of carbon nano-dots (CNDs) on structural and optical properties of PMMA polymer composite. *Results Phys.* **2019**, *15*, 102776. [[CrossRef](#)]
63. Abdullah, R.M.; Aziz, S.B.; Mamand, S.M.; Hassan, A.Q.; Hussein, S.A.; Kadir, M.F.Z. Reducing the crystallite size of spherulites in PEO-based polymer nanocomposites mediated by carbon nanodots and Ag nanoparticles. *Nanomaterials* **2019**, *9*, 874. [[CrossRef](#)]
64. Dhayal, V.; Upendra, S.Z.H.; Choudhary, K.B.L. Optical and electrical properties of biocompatible and novel (CS–GO) polymer nanocomposites. *Opt. Quantum Electron.* **2021**, *53*, 53. [[CrossRef](#)]
65. Taha, T.A. Optical properties of PVC/Al₂O₃ nanocomposite films. *Polym. Bull.* **2019**, *76*, 903–918. [[CrossRef](#)]
66. Alabdulaal, T.H.; Yahia, I.S. Optical linearity and nonlinearity, structural morphology of TiO₂-doped PMMA/FTO polymeric nanocomposite films: Laser power attenuation. *Optik* **2021**, *227*, 166036. [[CrossRef](#)]
67. Muhammed, D.S.; Brza, M.A.; Nofal, M.M.; Aziz, S.B.; Hussien, S.A.; Abdulwahid, R.T. Optical dielectric loss as a novel approach to specify the types of electron transition: XRD and UV-vis as a non-destructive techniques for structural and optical characterization of peo based nanocomposites. *Materials* **2020**, *13*, 2979. [[CrossRef](#)]
68. Aziz, S.B. Morphological and optical characteristics of chitosan_(1-x):Cu⁰_x (4 ≤ x ≤ 12) based polymer nano-composites: Optical dielectric loss as an alternative method for tauc's model. *Nanomaterials* **2017**, *7*, 444. [[CrossRef](#)] [[PubMed](#)]
69. Taha, T.A.; Hendawy, N.; El-Rabaie, S.; Esmat, A.; El-Mansy, M.K. Effect of NiO NPs doping on the structure and optical properties of PVC polymer films. *Polym. Bull.* **2019**, *76*, 4769–4784. [[CrossRef](#)]
70. Bhargav, P.B.; Mohan, V.M.; Sharma, A.K.; Rao, V.V.R.N. Structural, Electrical and Optical Characterization of Pure and Doped Poly (Vinyl Alcohol) (PVA) Polymer Electrolyte Films. *Int. J. Polym. Mater.* **2007**, *56*, 579–591. [[CrossRef](#)]
71. Irfan, M.; Manjunath, A.; Mahesh, S.S. Study on the optical properties of polyvinyl alcohol doped sodium fluoride polymer electrolyte films. *AIP Conf. Proc.* **2020**, *2220*, 80063. [[CrossRef](#)]
72. Abdullah, O.G.; Tahir, D.A.; Ahmad, S.S.; Ahmad, H.T. Optical Properties of PVA: CdCl₂. H₂O Polymer Electrolytes. *IOSR J. Appl. Phys.* **2013**, *4*, 52–57. [[CrossRef](#)]
73. Kiran, M.G.; Jyothi, N.K.; Samatha, K.; Rao, M.P.; Prasad, V.B.V.N. Studies on optical properties of Pva based complex polymer electrolyte. *RASAYAN J. Chem.* **2021**, *14*, 760–767. [[CrossRef](#)]
74. Sheha, E.; Khoder, H.; Shanap, T.S.; El-Shaarawy, M.G.; El Mansy, M.K. Structure, dielectric and optical properties of p-type (PVA/CuI) nanocomposite polymer electrolyte for photovoltaic cells. *Optik* **2012**, *123*, 1161–1166. [[CrossRef](#)]
75. Gh, O.; Aziz, S.B.; Rasheed, M.A. Structural and optical characterization of PVA: KMnO₄ based solid polymer electrolyte. *Results Phys.* **2016**, *6*, 1103–1108. [[CrossRef](#)]
76. Varishetty, M.M.; Qiu, W.; Gao, Y.; Chen, W. Structure, Electrical and Optical Properties of (PVA/LiAsF₆) Polymer Composite Electrolyte Films. *Polym. Eng. Sci.* **2010**, *50*, 878–884. [[CrossRef](#)]
77. Ali, H.E.; Algarni, H.; Yahia, I.S.; Khairy, Y. Optical absorption and linear / nonlinear parameters of polyvinyl alcohol films doped by fullerene. *Chin. J. Phys.* **2021**, *72*, 270–285. [[CrossRef](#)]
78. Ismail, A.M.; Mohammed, M.I.; Yahia, I.S. A facile method to prepare g-carbon nitride/poly (vinyl alcohol) nanocomposite films with remarkable optoelectrical properties: Laser attenuation approach. *Opt. Laser Technol.* **2021**, *134*, 106600. [[CrossRef](#)]
79. Taha, T.A.; Saleh, A. Dynamic mechanical and optical characterization of PVC/fGO polymer nanocomposites. *Appl. Phys. A Mater. Sci. Process.* **2018**, *124*, 600. [[CrossRef](#)]
80. Illya, N.; Fauzi, M.; Fen, Y.W.; Abdullah, J.; Kamarudin, M.A.; Alia, N.; Omar, S.; Bashar, F.; Eddin, K.; Ramdzan, N.S. Evaluation of Structural and Optical Properties of Graphene Oxide–Polyvinyl Alcohol Thin Film and Its Potential for Pesticide Detection Using an Optical Method. *Photonics* **2022**, *9*, 300. [[CrossRef](#)]
81. Soliman, T.S.; Vshivkov, S.A. Effect of Fe nanoparticles on the structure and optical properties of polyvinyl alcohol nanocomposite films. *J. Non. Cryst. Solids* **2019**, *519*, 119452. [[CrossRef](#)]
82. Yahia, I.S.; Mohammed, M.I.; Nawar, A.M. Multifunction applications of TiO₂/poly(vinyl alcohol) nanocomposites for Laser attenuation applications. *Phys. B Phys. Condens. Matter* **2018**, *556*, 48–60. [[CrossRef](#)]
83. Sabry, N.; Mohammed, M.I.; Yahia, I.S. Optical analysis, optical limiting and electrical properties of novel PbI₂/PVA polymeric nanocomposite films for electronic optoelectronic applications. *Mater. Res. Express* **2019**, *6*, 115339. [[CrossRef](#)]
84. Gh, O.; Shujahadeen, A.; Khalid, B.A.; Yousif, M.O. Reducing the optical band gap of polyvinyl alcohol (PVA) based nanocomposite. *J. Mater. Sci. Mater. Electron.* **2015**, *26*, 5303–5309. [[CrossRef](#)]
85. Vedhavathi, H.S.; Divya, U.S.; Madhukar, B.S.; Vanga, P.R.; Swamy, N.K. PVA/Gd₂O₃@Zno Nanocomposite Films as New Uv-Blockers: Structure and Optical Revealations. *J. Inorg. Organomet. Polym. Mater.* **2021**, *32*, 1853–1867. [[CrossRef](#)]
86. Ali, H.E.; Yahia, I.S.; Algarni, H.; Khairy, Y. Enhancing the optical absorption, conductivity, and nonlinear parameters of PVOH films by Bi-doping. *N. J. Phys.* **2021**, *23*, 43001. [[CrossRef](#)]
87. Abdullah, O.G.; Salh, D.M.; Mohamad, A.H.; Jamal, G.M.; Ahmed, H.T.; Mustafa, B.S.; Suhail, M.H. Linear and nonlinear optical characterization of dye–polymer composite films based on methylcellulose incorporated with varying content of methylene blue. *J. Electron. Mater.* **2022**, *51*, 675–683. [[CrossRef](#)]

88. Mostafa, M.Y.A.; Zakaly, H.M.H.; Issa, S.A.M.; Saudia, H.A.; Henaish, A.M.A. Tailoring variations in the linear optical and radiation shielding parameters of PVA polymeric composite films doped with rare-earth elements. *Appl. Phys. A* **2022**, *128*, 199. [[CrossRef](#)]
89. Ismail, M.S.; Elamin, A.A.; Abdel-Wahab, F.; Elbasha, Y.H.; Mahasen, M.M. Improving the refractive index by engineering PbS/PVA nano polymer composite for optoelectronic applications. *Opt. Mater.* **2022**, *131*, 112639. [[CrossRef](#)]
90. Ahmed, B.Y.; Rashid, S.O. Synthesis, characterization, and application of metal-free sulfonamide-vitamin C adduct to improve the optical properties of PVA polymer. *Arab. J. Chem.* **2022**, *15*, 104096. [[CrossRef](#)]
91. Saeed, C.O.; Qader, A.A.; Aziz, S.B.A. Low cost novel PEO based nano-composite for semiconductor and He-Ne lasers beam attenuation: Structural and optical properties. *Opt. Mater.* **2022**, *129*, 112502. [[CrossRef](#)]
92. Darwesh, A.H.; Aziz, S.B.; Hussien, S.A. Insights into optical band gap identification in polymer composite films based on PVA with enhanced optical properties: Structural and optical characteristics. *Opt. Mater.* **2022**, *133*, 113007. [[CrossRef](#)]
93. Yu, L.; Li, D.; Zhao, S.; Li, G.; Yang, K. First principles study on electronic structure and optical properties of ternary GaAs:Bi alloy. *Materials* **2012**, *5*, 2486–2497. [[CrossRef](#)]
94. Hossain, F.M.; Sheppard, L.; Nowotny, J.; Murch, G.E. Optical properties of anatase and rutile titanium dioxide: Ab initio calculations for pure and anion-doped material. *J. Phys. Chem. Solids* **2008**, *69*, 1820–1828. [[CrossRef](#)]
95. Brza, M.A.; Aziz, S.B.; Anuar, H.; Ali, F.; Dannoun, E.M.A.; Saeed, S.R.; Mohammed, S.J.; Abdulwahid, R.T. Green coordination chemistry as a novel approach to fabricate polymer: Cd(II)-complex composites: Structural and optical properties. *Opt. Mater.* **2021**, *116*, 111062. [[CrossRef](#)]
96. Lü, C.; Guan, C.; Liu, Y.; Cheng, Y.; Yang, B. PbS/Polymer Nanocomposite Optical Materials with High Refractive Index. *Chem. Mater.* **2005**, *17*, 2448–2454. [[CrossRef](#)]

Disclaimer/Publisher's Note: The statements, opinions and data contained in all publications are solely those of the individual author(s) and contributor(s) and not of MDPI and/or the editor(s). MDPI and/or the editor(s) disclaim responsibility for any injury to people or property resulting from any ideas, methods, instructions or products referred to in the content.